# A MULTIGRID METHOD FOR ELASTIC SCATTERING*

JAN MANDEL AND MIRELA POPA†

September 1997
Updated January 1998

**Abstract.** A finite element discretization and a multigrid method for an acoustic elastodynamic model are presented. The model problem is a channel with rigid walls and elastic obstacle in the middle, Dirichlet boundary condition for the incoming wave, Neumann boundary conditions at rigid surfaces on the sides, and an absorbing boundary at the outgoing side. The discrete solutions appear to converge as $O(h^2)$. The discretization is verified by comparing discrete solutions with known analytic solutions for a modified problem. An efficient V-cycle multigrid algorithm is developed to solve the discrete equations. The method employs smoothing by iterating on the squared system, combined with a block Jacobi step to resolve variables in a neighborhood of the interface. The efficiency of the method is demonstrated on numerical experiments.

**1. Introduction.** Multigrid methods for the solution of the Helmholtz equation of acoustic in scattering are classical [3, 4]; for more recent development, see [5, 8]. However, multigrid methods for the coupled acoustic-elastic problem do not seem to have been investigated. In this paper, we formulate such method and present preliminary numerical experience from a prototype implementation in MATLAB.

**2. Formulation of the problem.** Consider situation as in Fig. 2.1. The domain $\Omega_f$ is filled with fluid, with elastic obstacle $\Omega_e$, and interface $\Gamma_i$.

The acoustic field in the fluid is governed by the Helmholtz equation for the pressure $p$,

$$\Delta p + K^2 p = 0 \quad \text{in} \quad \Omega_e, \tag{2.1}$$

with the boundary conditions

$$\begin{aligned} p &= p_0 \quad \text{on} \quad \Gamma_d \quad \text{(excitation)}, \\ \frac{\partial p}{\partial \mathbf{n}} &= 0 \quad \text{on} \quad \Gamma_n \quad \text{(sound hard surface)}, \\ \frac{\partial p}{\partial \mathbf{n}} + iKp &= 0 \quad \text{on} \quad \Gamma_a \quad \text{(radiation boundary condition)}. \end{aligned}$$

The acoustic field in the isotropic elastic medium satisfies equation

$$\nabla \cdot \tau + \omega^2 \rho_e u = 0 \quad \text{in} \quad \Omega_e, \tag{2.2}$$

where

$$\begin{aligned} \tau &= \lambda I(\nabla \cdot u) + 2\mu e(u) && \text{is the stress tensor,} \\ e_{ij}(u) &= \tfrac{1}{2}\left(\tfrac{\partial u_i}{\partial x_j} + \tfrac{\partial u_j}{\partial x_i}\right) && \text{is the strain tensor,} \end{aligned}$$

$u$ is the displacement, $\rho_e$ is the density, and $\lambda$ and $\mu$ are the Lamé coefficients of the elastic medium.

*This research was supported by the Office of Naval Research under grant N-00014-95-1-0663. This is an interim work report. A modified version of this report will be submitted for publication in future.

†Department of Mathematics, University of Colorado at Denver, Denver, CO 80217-3364

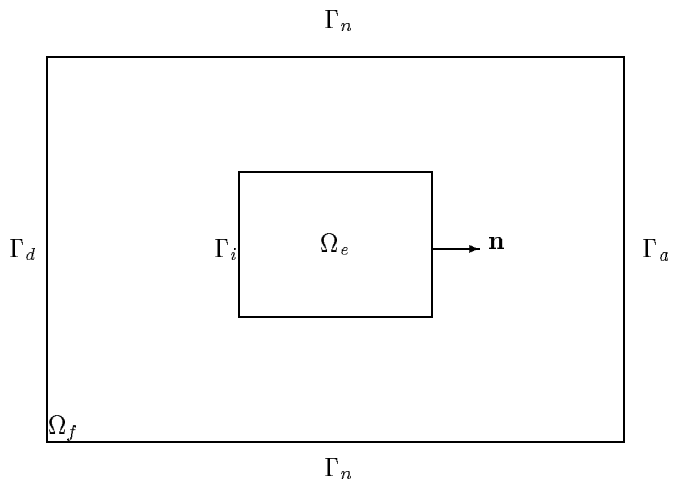

FIG. 2.1. *Problem setup*

The solid-fluid interface conditions are [9]

$$\left.\begin{array}{rcll} \mathbf{n}\cdot u &=& \frac{1}{\rho_f\omega^2}\frac{\partial p}{\partial \mathbf{n}} & \text{(continuity)} \\ \mathbf{n}\cdot\tau\cdot\mathbf{n} &=& -p & \text{(balance of normal forces)} \\ \mathbf{n}\times\tau\cdot\mathbf{n} &=& 0 & \text{(zero tangential tension)} \end{array}\right\} \quad \text{on} \quad \Gamma_i$$

**3. Variational Form and FE Discretization.** Define the spaces

$$V_f = \{q \in \mathbf{H}^1(\Omega_f) | q = 0 \quad \text{on} \quad \Gamma_d\},$$
$$V_e = \{u \in (\mathbf{H}(\Omega_e))^3\}.$$

Multiplying equation (2.1) by a test function $q \in V_f$, equation (2.2) by a test function $u \in V_e$, and integrating by parts over $\Omega$ we obtain the following variational form of (2.1), (2.2), and (2): Find $p$, $p - p_0 \in V_f$ and $u \in V_e$ such that

$$-\int_{\Omega_f} \nabla p \nabla q + K^2 \int_{\Omega_f} pq - iK \int_{\Gamma_a} pq - \int_{\Gamma} \rho_f \omega^2 (\mathbf{n}\cdot u) q = 0 \tag{3.1}$$

$$-\int_{\Omega_e} \lambda(\nabla\cdot u)(\nabla\cdot v) + 2\mu e(u) : e(v) + \omega^2 \int_{\Omega_e} \rho_e u\cdot v - \int_{\Gamma} p(\mathbf{n}_e\cdot v) = 0 \tag{3.2}$$

$$\forall q \in V_f \quad \text{and} \quad \forall v \in V_e,$$

where $p_0$ on $\Gamma_d$ is understood to be extended to a function in $H^1(\Omega_f)$. Replacing $V_f$ and $V_e$ with conforming finite element spaces, we obtain the algebraic system

$$\begin{pmatrix} -\mathbf{K}_f + K^2\mathbf{M}_f - iK\mathbf{G}_f & -\rho_f\omega^2\mathbf{T} \\ -\mathbf{T}^t & -\mathbf{K}_e + \omega^2\mathbf{M}_e \end{pmatrix} \begin{pmatrix} \tilde{p} \\ \tilde{u} \end{pmatrix} = R \tag{3.3}$$

In the coupled system (3.3), $\tilde{p}$ and $\tilde{u}$ are the algebraic representations of $p$ and $u$, i.e., $p$ and $u$ are the finite element interpolations of $\tilde{p}$ and $\tilde{u}$, respectively. The matrix blocks in (3.3) are defined by

$$\tilde{p}^t \mathbf{K}_f \tilde{q} = \int_{\Omega_f} \nabla p \nabla q,$$

| $h = \frac{1}{10}$ | $h = \frac{1}{20}$ | $h = \frac{1}{40}$ |
|---|---|---|
| -0.8659 - 0.7108i | -0.8883 - 0.6988i | -0.8946 - 0.6953i |
| -0.8659 - 0.7108i | -0.8883 - 0.6988i | -0.8946 - 0.6953i |
| 0.1802 + 1.0028i | 0.2198 + 0.9998i | 0.2298 + 0.9982i |
| 0.1802 + 1.0028i | 0.2198 + 0.9998i | 0.2298 + 0.9982i |
| -0.1172 + 0.1477i | -0.1139 + 0.1512i | -0.1129 + 0.1519i |
| 0.0000 + 0.0000i | 0.0000 + 0.0000i | 0.0000 + 0.0000i |
| $h = \frac{1}{80}$ | $h = \frac{1}{160}$ | $h = \frac{1}{320}$ |
| -0.8964 - 0.6943i | -0.8969 - 0.6940i | -0.8971 - 0.6940i |
| -0.8964 - 0.6943i | -0.8969 - 0.6940i | -0.8971 - 0.6940i |
| 0.2323 + 0.9976i | 0.2329 + 0.9974i | 0.2330 + 0.9973i |
| 0.2323 + 0.9976i | 0.2329 + 0.9974i | 0.2330 + 0.9973i |
| -0.1126 + 0.1519i | -0.1125 + 0.1519i | -0.1125 + 0.1519i |
| 0.0000 + 0.0000i | 0.0000 + 0.0000i | 4.6715e-13 + 3.5061e-13i |

TABLE 4.1
*Solution Convergence on 6 sample points (Fig.4.1), $K = 5$*

$$\tilde{p}^t \mathbf{M}_f \tilde{q} = \int_{\Omega_f} pq,$$

$$\tilde{p}^t \mathbf{G}_f \tilde{q} = \int_{\Gamma_a} pq,$$

$$\tilde{u}^t \mathbf{K}_e \tilde{v} = \int_{\Omega_e} \lambda(\nabla \cdot u)(\nabla \cdot v) + 2\mu e(u) : e(v),$$

$$\tilde{u}^t \mathbf{M}_e \tilde{v} = \omega^2 \int_{\Omega_e} \rho_e u \cdot v,$$

$$\tilde{p}^t \mathbf{T} \tilde{v} = \int_{\Gamma} p(\mathbf{n} \cdot v).$$

The right-hand side $R$ of the system (3.3) is defined from the zero right hand side of the variational form with the modification for the Dirichlet boundary condition $p = p_0$ on $\Gamma_d$ as follows. Listing the the degrees of freedom on $\Gamma_d$ firts and the remaining variables as second, (3.3) becomes $AU = R$, where the solution, the right hand side, and the matrix are, respectively,

$$U = \begin{pmatrix} U_1 \\ U_2 \end{pmatrix}, \qquad R = \begin{pmatrix} R_1 \\ R_2 \end{pmatrix}, \qquad A = \begin{pmatrix} A_{11} & A_{12} \\ A_{21} & A_{22} \end{pmatrix}.$$

Here, $R_1$ are the degrees of freedom for $p_0$, and $R_2 = 0$. We impose the constraint $U_1 = R_1$ and solve for $U_2$ from the equations in second block, which gives the system of equation that is actually solved,

$$\begin{pmatrix} I & 0 \\ 0 & A_{22} \end{pmatrix} \begin{pmatrix} U_1 \\ U_2 \end{pmatrix} = \begin{pmatrix} R_1 \\ -A_{21} R_1 \end{pmatrix}$$

**4. Numerical Verification of the Discretization.** In all computational examples, the size of the domain in the $x$ and $y$-direction was chosen to be always

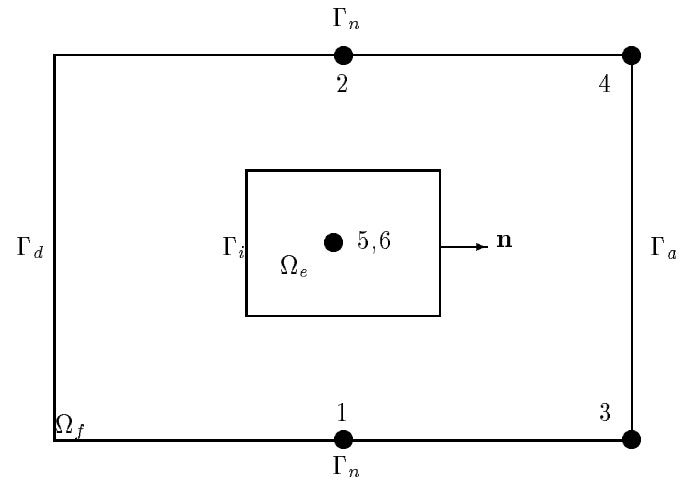


FIG. 4.1. *Configuration of sample points for table 4.1. Sample points 1,2,3,4 are fluid pressure values, and sample points 5,6 are $u_x$ and $u_y$ displacements, respectively.*

| test | p | $u_x$ | $u_y$ | comment |
|---|---|---|---|---|
| a | $e^{iKx}$ | 0 | 0 | pressure wave in $x$ direction |
| b | $e^{iKy}$ | 0 | 0 | pressure wave in $y$ direction |
| c | 0 | $e^{-ic_px}$ | 0 | compression wave in $x$ direction |
| d | 0 | 0 | $e^{-ic_py}$ | compression wave in $y$ direction |
| e | 0 | 0 | $e^{-ic_sx}$ | shear wave in $x$ direction |
| f | 0 | $e^{-ic_sy}$ | 0 | shear wave in $y$ direction |

TABLE 4.2
*Summary of comparisons with analytic solution*

1. The obstacle in the channel is setup in the middle as a square of size 0.2, cf., Fig. 2.1. The boundary condition on $\Gamma_d$ was $p_0(x, y) = \sin(\pi y)$, assuming the origin of the coordinates in the lower left corner of $\Omega$. The fluid medium was water with the density $\rho_f = 1000kg\,m^{-3}$ and the speed of sound $c_f = 1500m\,s^{-1}$. The elastic medium was aluminum with the density $\rho_e = 2700kg\,m^{-3}$, the Lamé coefficient $\mu = 10^{10} \cdot 2.6N\,m^{-2}$, and the speed of sound $c_p = 6300m\,s^{-1}$ for pressure waves and $c_s = 3100m\,s^{-1}$ for shear waves. Standard $Q_1$ finite element basis functions were used for the discretization.

The problem (3.3) was solved directly using sparse LU decomposition in MATLAB with SYMRCM reordering to reduce the profile bandwidth of the matrix. Table 4.1 demonstrates the convergence of the solution. The wave number was chosen to be $K = 5$. The results are values at sample points for different mesh sizes, from $10 \times 10$ to $320 \times 320$. The values appear to converge about as $0(h^2)$, as expected. The solution is displayed in Fig. 4.2.

The discretization was further tested by comparison of numerical and analytical solutions. Since we do not know analytic solutions to coupled problems, we prescribe the solution in $\Omega_e$ and $\Omega_f$ as planar waves and modify the right hand side of the interface condition (2) so that the coupled system (3.1), (3.2) has this solution. Table 4.2 contains a summary of the analytic tests the solution was compared to, namely pressure waves and shear waves. Here the wave speeds $c_p$ and $c_s$ satisfy $c_p = \sqrt{(\lambda + 2\mu)/\rho_e}$ and $c_s = \sqrt{\mu/\rho_e}$.

The numerical results are summarized in table 4.3. This table shows the decrease

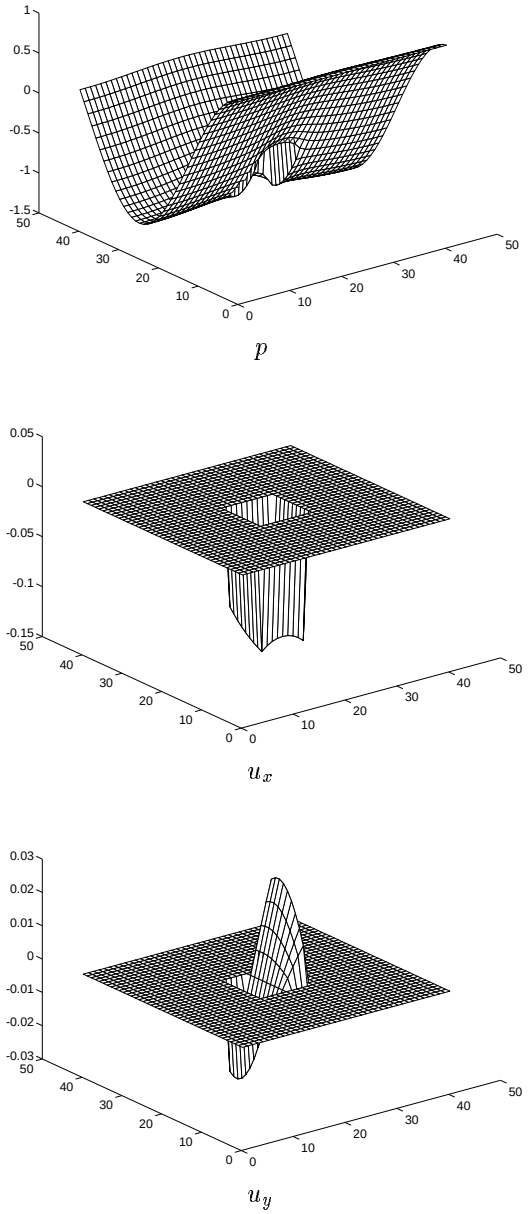


FIG. 4.2. *Solution for a 40 × 40 mesh and $K = 5$ and right hand side modified for the Dirichlet boundary condition $p = p_0$ on $\Gamma_d$*

of the error for different mesh sizes. The error is expected to decrease as $O(h^2)$. However, the observed error appears to decrease only as $0(h)$. This is probably caused by the discretization of the artificial right hand side at the interface by integration with finite element test functions.

To test the solution accuracy without artificial right hand sides at the interface, we have changed the setup of the problem by changing the size of the obstacle. The

TABLE 4.3
*Maximum difference between analytic and finite element solution for artificial right hand sides at the interface*

| test | 10 × 10 | 20 × 20 | 40 × 40 | 80 × 80 | 160 × 160 |
|---|---|---|---|---|---|
| a | 0.0377 | 0.0057 | 7.5966e-04 | 9.7454e-05 | 1.2325e-05 |
| b | 0.0377 | 0.0057 | 7.5966e-04 | 9.7454e-05 | 1.2325e-05 |
| c | 0.2395 | 0.0999 | 0.0450 | 0.0212 | 0.0103 |
| d | 0.2395 | 0.0999 | 0.0450 | 0.0212 | 0.0103 |
| e | 2.4967e-05 | 2.6033e-06 | 2.9294e-07 | 3.4586e-08 | 4.1961e-09 |
| f | 2.4967e-05 | 2.6033e-06 | 2.9294e-07 | 3.4586e-08 | 4.1961e-09 |

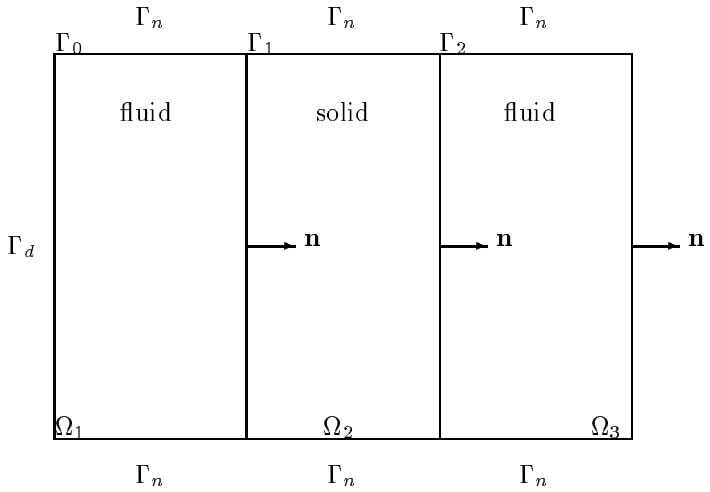


FIG. 4.3. *Sound penetration through a wall*

obstacle was extended from one Neumann boundary to the other as it can be seen in Fig. 4.3. In this way the exact solution could be calculated directly and it was compared to the solution obtained from the discretization. The exact solution had to meet the following conditions:

$$
\begin{aligned}
p(0,y) &= 1 \quad \text{on} \quad \Gamma_0 \\
u_x &= \frac{-ik}{\rho_f \omega^2} e^{-ikx_1} \quad \text{on} \quad \Gamma_1 \text{ and } \Gamma_2 \\
\tau \cdot \mathbf{n} + p\mathbf{n} &= 0 \quad \text{on} \quad \Gamma_1 \text{ and } \Gamma_2 \\
p &= e^{-ikx} \quad \text{on} \quad \Omega_1 \\
u_y &= 0 \quad \text{on} \quad \Omega_2 \\
u_x &= ae^{-i\frac{\omega}{c_p}x} + ce^{i\frac{\omega}{c_p}x} \quad \text{on} \quad \Omega_2 \\
p &= de^{-ikx_2} \quad \text{on} \quad \Omega_3
\end{aligned}
$$

Imposing these conditions, the constants a,c,d were found, giving an analytic solution. Fig. 4.4 displays the residue of the exact solution. The error is concentrated at the upper and lower boundary, where a natural boundary condition was implemented; this condition is not appropriate for modeling an infinite slab.

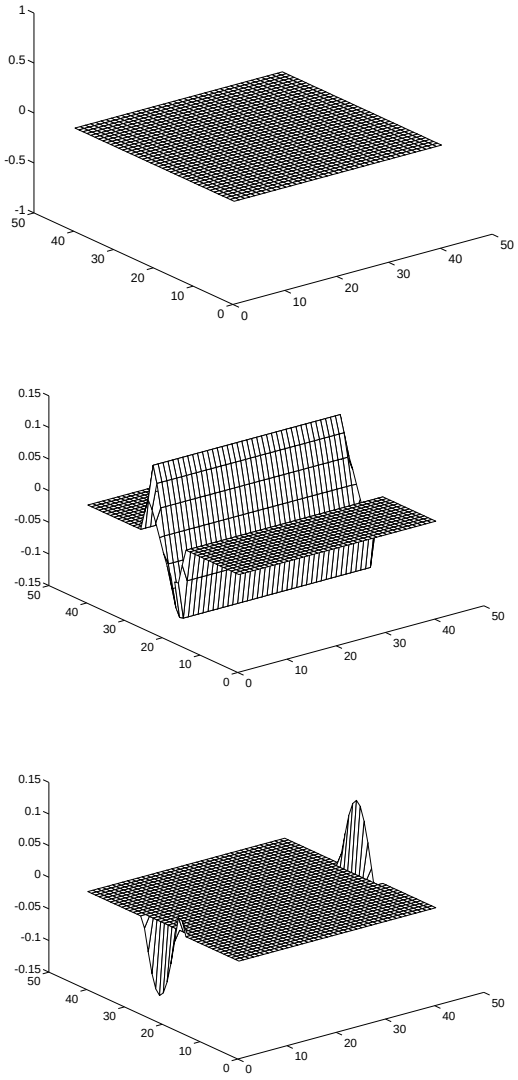


FIG. 4.4. *Residual of exact solution for a $40 \times 40$ mesh and $K = 5$ and right hand side modified for the Dirichlet boundary condition $p = p_0$ on $\Gamma_d$, and Neumann boundary conditions implemented at the solid-fluid interface instead of interface conditions.*

**5. Multigrid Approach.** We have developed a multigrid algorithm to solve the coupled problem (3.3). Standard geometric coarsening and prolongations and restrictions based on the finite element space were used. The interface was always on the mesh boundary of the coarse mesh. The coarse matrices were created variationally.

It turned out that the the key to satisfactory multigrid performance is the design of suitable smoothing. As the basic smoother, we have used Jacobi iterations on squared diagonally preconditioned system; this guarantees that the smoothing is a convergent iterative process, makes the overall multigrid process more stable, and

allows to increase the number of smoothing steps when necessary. This version of the multigrid method converged well when applied to each part of the coupled problem separately, but convergence for the whole coupled problem was very slow. Inspired by the well known fact that additional smoothing in the neighborhood of boundaries is beneficial in multigrid [1], we have added a block Jacobi iteration step with one large block that contains all variables on the interface and all nodes anjacent to the interface. Satisfactory convergence was not obtained with a smaller block.

Specifically, the essential ingredients of the multigrid algorithm are as follows. First, matrix $A$ in problem (3.3) was symmetrized as follows:

$$A \leftarrow \begin{pmatrix} aI & 0 \\ 0 & I \end{pmatrix} A \begin{pmatrix} \frac{1}{a}I & 0 \\ 0 & I \end{pmatrix}$$

where $a = \frac{1}{\omega\sqrt{\rho_f}}$ and $I$ stands for the identity matrix, and 0 represents 0 matrices. Two matrices $D$ and $\tilde{D}$ of the same size as $A$ were created for the smoothing algorithm. $D$ consists of the submatrix of $A$ corresponding to degrees of freedom of the interface, of the nodes adjacent to the interface in the pressure, and in the elastic part, embedded in the zero matrix of the same size as $A$. The matrix $\tilde{D}$ is block diagonal with $3 \times 3$ blocks corresponding to nodes. Using these matrices, one smoothing step is defined by

$$x \leftarrow x - (D^{-1} + \omega(\tilde{D}^{-1}A)^*\tilde{D}^{-1})(Ax - b).$$

The parameter $\omega$ was chosen as $\omega = 1/\lambda$, where $\lambda$ was obtained by several steps of the power method:

$$\lambda = \frac{< \tilde{D}^{-1}Au, \tilde{D}^{-1}Au >}{< u, u >}$$
$$u \leftarrow (\tilde{D}^{-1}A)^*(\tilde{D}^{-1}A)u$$

The problem on the coarsest level was solved directly.

**6. Computational Results with Multigrid.** The problem setup is same as in Section 4 above. The graph of the error in several iterations of a two-level method is in Fig. 6.1. The error was essentially at machine precision after one cycle already.

Observed convergence factors of one multigrid cycle are summarized in Table 6.1. It is clearly seen that convergence requires that the coarsest level is fine enough for the wave number $K$, and that more smoothing steps has a stabilizing effect on the iterations.

**7. Conclusion.** We have implemented a prototype of a finite element method for acoustic scattering in coupled fluid-solid system. The finite element solution was observed to converge as $0(h^2)$. However, the rate of $0(h)$ was seen in comparison with artificial problems with analytic solutions. A theoretical analysis is needed.

A multigrid method for the resulting discrete system was developed. This method is very efficient but it shares a common feature of multigrid for the Helmholtz equation, namely, the coarsest level has to be fine enough to capture the wave character of the problem [4]. One possible direction of future research is to adapt the use of planar wave functions [5] to the interface problem considered. Finally, infinite regions modeled by an integral boundary condition on a bounded region need to be considered.

REFERENCES

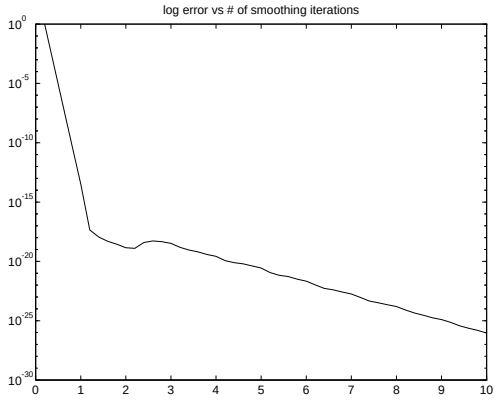


FIG. 6.1. *Decrease of the error after 10 multigrid cycles.* $40 \times 40$ *mesh,* $K = 5$*, two levels.*

| Five smoothing steps per level | | | | |
|---|---|---|---|---|
| level | h | $K = 5$ | $K = 10$ | $K = 20$ |
| 2 | $\frac{1}{16}$ | 2.898e-08 | 1.411e-07 | 1.11e+06 |
| 3 | $\frac{1}{32}$ | 7.5238e-08 | 7.757e-05 | 5.2442e+7 |
| 4 | $\frac{1}{64}$ | 1.308e-07 | 7.515e-05 | 1.901e+8 |
| 5 | $\frac{1}{128}$ | 2.839e-07 | 2.560e-05 | 5.258e+8 |
| Two smoothing steps per level | | | | |
| level | h | $K = 5$ | $K = 10$ | $K = 20$ |
| 2 | $\frac{1}{16}$ | 5.219e-07 | 2.901e-06 | 1.391e+09 |
| 3 | $\frac{1}{32}$ | 7.515e-05 | 3.708e-04 | 8.816e+48 |
| 4 | $\frac{1}{64}$ | 5.736603e-05 | 1.117369e+21 | 4.029064e+49 |
| 5 | $\frac{1}{128}$ | 1.009e-05 | 2.5617e+22 | 8.6271e+49 |
| Five smoothing steps per level | | | | |
| level | h | $K = 5$ | $K = 10$ | $K = 20$ |
| 2 | $\frac{1}{128}$ | 8.848e-08 | 2.024e-05 | 0.01177 |
| 3 | $\frac{1}{128}$ | 2.86e-07 | 9.775e-05 | 0.03155 |
| 4 | $\frac{1}{128}$ | 2.924e-07 | 5.406e-05 | 0.6266 |
| 5 | $\frac{1}{128}$ | 2.839e-07 | 2.560e-05 | 5.258e+8 |
| 6 | $\frac{1}{128}$ | 1.949e-07 | 1.163e-05 | 5.21e+9 |

TABLE 6.1
*Residual Reduction Factors of one Multigrid Cycle in the* $l^2$ *norm*

[1] A. BRANDT, *Multigrid techniques: 1984 guide with applications to fluid dynamics*, GMD–Studien Nr. 85, Gesellschaft für Mathematik und Datenverarbeitung, St. Augustin, 1984.

[2] P. G. CIARLET, *Mathematical Analysis of the Finite Element Method*, Academic Press, New York, 1972.

[3] C. I. GOLDSTEIN, *Multigrid preconditioners applied to the iterative solution of singularly perturbed elliptic boundary value problems and scattering problems*, in Innovative numerical methods in engineering, Proc. 4th Int. Symp., Atlanta/Ga., 1986, R. Shaw, J. Periaux, A. Chaudouet, J. Wu, C. Marino, and C. Brebbia, eds., Berlin, 1986, Springer-Verlag, pp. 97–102.

[4] W. HACKBUSCH, *A fast iterative method for solving Helmholtz's equation in a general region*, in Fast Elliptic Solvers, U. Schumann, ed., Advance Publications, London, 1978, pp. 112–124.

[5] B. Lee, T. Manteuffel, S. McCormick, and J. Ruge, *Multilevel first-order system least squares (FOSLS) for Helmholtz equation*, in Procs. 2nd International Conf. on Approx. and Num. Meths. for the Solution of the Maxwell Equations, Washington, D.C, John Wiley and Sons, 1993.

[6] R. W. Lewis, P. Bettess, and E. Hinton, *Numerical Methods in Coupled Systems*, John Wiley & Sons, 1984.

[7] J. Mandel, S. McCormick, and R. Bank, *Variational multigrid theory*, in Multigrid Methods, S. F. McCormick, ed., SIAM, Philadephia, 1987, ch. 5, pp. 131–177.

[8] P. Vaněk, J. Mandel, and M. Brezina, *Solving a two-dimensional Helmholtz problem by algebraic multigrid*, UCD/CCM Report 110, Center for Computational Mathematics, University of Colorado at Denver, October 1997. http://www-math.cudenver.edu/ccmreports/rep110.ps.gz.

[9] V. Varadan and V. Varadan, *Acoustic, electromagnetic, and elastodynamic fields*, in Field Representations and Introduction to Scattering, V. Varadan and V. Varadan, eds., North-Holland, Amsterdam, 1991.